Limnol. Oceanogr., 56(5), 2011, 1866–1878

doi:10.4319/lo.2011.56.5.1866

Trophic cycling and carbon export relationships in the California Current Ecosystem

Michael R. Stukel,[a,*,1] Michael R. Landry,[a] Claudia R. Benitez-Nelson,[b] and Ralf Goericke[a]

[a] Scripps Institution of Oceanography, University of California at San Diego, La Jolla, California
[b] Marine Science Program & Department of Earth and Ocean Sciences, University of South Carolina, Columbia, South Carolina

Abstract

We constructed a simple non–steady-state model of trophic cycling relationships in the California Current Ecosystem and tested its predictions of mesozooplankton fecal-pellet export against vertical carbon-flux measurements by the ^{234}Th method taken during Lagrangian experiments. To assess trophic relationships, we simultaneously measured ^{14}C-primary production and chlorophyll-based rate estimates of phytoplankton growth, microzooplankton grazing, mesozooplankton grazing, and net phytoplankton growth. Study locations ranged from coastal upwelling to offshore oligotrophic conditions. *E*-ratios (carbon export : ^{14}C-primary production) predicted by the model ranged from 0.08 to 0.14, in good agreement with both the magnitude and the variability found in contemporaneous measurements of ^{234}Th export and C : ^{234}Th-ratios of sinking particles. *E*-ratios were strongly decoupled from new production estimates. The lowest measured and predicted *e*-ratios were associated with higher nutrient chlorophyll parcels with net accumulating phytoplankton in the inshore region. For our study sites, variability in export efficiency was determined by the local net balance of growth and grazing and the relative strengths of grazing pathways to microzooplankton and mesozooplankton. Despite very different plankton assemblages studied, the consistently good agreement between independently measured production-grazing processes and biogeochemical rates suggest that zooplankton are the major drivers of vertical carbon-flux in this system during springtime.

The vertical export of particulate carbon from the surface to the deep ocean is a critical component of the ocean's carbon cycle. Although much is known about the general patterns of export and their relationships to ecosystem properties over large regions of the open ocean (Buesseler 1998), our understanding of such fluxes in coastal regions and mechanisms controlling these is relatively limited. Because coastal regions typically have high rates of new and primary production on an areal basis, they likely play disproportionate roles in global carbon cycling and export (Eppley and Peterson 1979). The biologically mediated processes that drive export may also vary among and within coastal regions, from sinking phytodetritus (Green and Sambrotto 2006) to fecal-pellet flux (Landry et al. 1994; Umani et al. 2002), with varying additional effects of the physiological state of phytoplankton, inorganic ballasting (Armstrong et al. 2002), and aggregation processes (Alldredge and Gotschalk 1989; Walsh and Gardner 1992; Jackson 2001). Studies are, thus, needed that link measured ecological rates to vertical carbon-flux measurements across the range of conditions that define coastal ecosystems.

Coastal regions can be strongly advective systems, where production and export processes are often uncoupled. Lagrangian sampling schemes that allow simultaneous measurement of ecosystem processes, net community changes, and biogeochemical fluxes, thus have significant advantages for coastal studies. Landry et al. (2009), for instance, used a Lagrangian strategy to investigate phytoplankton rate relationships across a spectrum of ecological conditions and biotic communities in the California Current Ecosystem (CCE), finding that measured depth-integrated growth and grazing rates explained > 90% of the variability in the observed net growth rates of ambient phytoplankton over the duration of 3–5-d experiments. This good agreement between observed and predicted net changes based only on growth rate estimates and grazing losses to micro- and mesozooplankton suggested that direct sinking of phytoplankton out of the euphotic zone contributed surprisingly little, on average, to the temporal dynamics of phytoplankton. Here, we use data from four widely varying water parcels sampled in May 2006 of that study to ask a related question—are experimental measurements of growth and grazing rates sufficient to explain the magnitude and pattern of export flux in this coastal system, without consideration of direct phytoplankton cell sinking? To answer this question, we develop a simple trophic model for computing carbon export estimates from experimental process rates, which we then test against independent measurements of export flux based on the ^{234}Th : ^{238}U disequilibrium method (Buesseler et al. 1992). The underlying hypothesis in this comparison is that variability in vertical carbon flux in the CCE can be largely explained by the fluxes along trophic pathways that lead to fecal-pellet production of mesozooplankton. Alternatively, significant underprediction of export rates from the trophic model would be a strong indication that direct sinking of unconsumed phytoplankton, or other unmeasured processes, contribute substantially to the signal. Direct cell sinking and grazing losses to micro- and mesozooplankton are each coupled to export with very different efficiencies; therefore, our results highlight the importance of including a

* Corresponding author: mstukel@hpl.umces.edu

[1] Present address: Horn Point Laboratory, University of Maryland Center for Environmental Science, Cambridge, Maryland

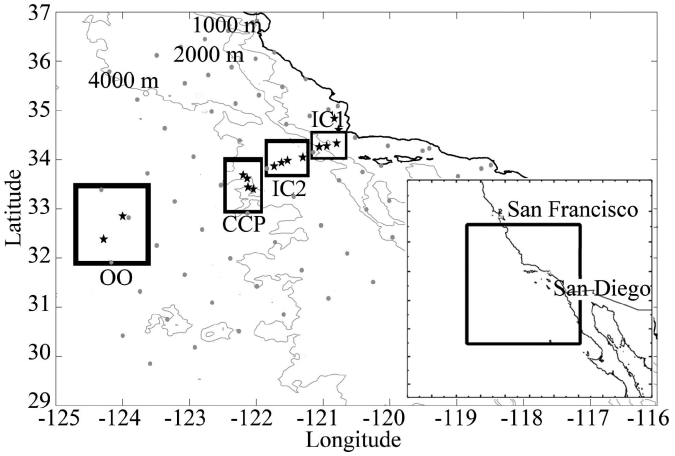

Fig. 1. Map of the study region. The stars show the locations of all ^{234}Th profiles, while the rectangles represent the four locations at which experimental cycles were conducted (OO, oligotrophic offshore, 01–05 Jun; CCP, California Current Proper, 16–21 May; IC1 and IC2, inshore cycles 1 and 2, 11–15 May and 26–31 May, respectively). Light gray dots show standard CalCOFI sampling stations in the area. Contour lines for seafloor depths of 1000, 2000, and 3000 m are graphed in gray. Inset at bottom right shows the study area (black rectangle) within the context of the southwestern coast of North America.

mechanistic understanding of ecological process rates and interactions in biogeochemical flux models. Our results also illustrate the strongly advective and unbalanced nature of the CCE upwelling ecosystem, where contemporaneous export is significantly lower than the expected rate of new production.

Methods

Overview of Lagrangian design—The study area (Fig. 1) was principally along historical sampling Line 80 of the California Cooperative Oceanic Fisheries Investigations (CalCOFI) Program, extending from the upwelling region off of Point Conception, California to nutrient-depleted offshore waters. For water parcels chosen to exploit the onshore–offshore range of ecosystem variability, a Lagrangian experimental approach was used to investigate relationships between measured rates of trophic interactions and vertical carbon flux. As described by Landry et al. (2009), individual experiments were initiated in homogenous surface-water parcels, identified and surveyed with a combination of satellite imagery and underway surveys with a Moving Vessel Profiler system (MVP; M. D. Ohman unpubl.). Water parcels were drogued with a drift array that included a 3 × 1-m holey-sock drogue centered at 15-m depth, a surface float equipped with Globalstar satellite communications, and a line below with attachments for in situ bottle incubations to assess growth, production, and grazing rates of the phytoplankton community. Sampling and experimental studies were conducted daily while tracking the water parcels for the duration of an experimental cycle (typically, 4 d). This strategy provided estimates of the net observed changes in the ambient phytoplankton community concurrently with the experimentally determined rates of production and grazing, which we use below for trophic modeling. To estimate vertical carbon flux, we measured water-column ^{234}Th deficiency and C : ^{234}Th-ratios on either 35–75-μm or 20–75-μm particles at specific depths within the same water parcels.

Four experimental cycles were conducted; two inshore parcels of recent and aged upwelled water (inshore Cycles 1 and 2, respectively), one in the low-salinity core of the California Current proper, and one in offshore oligotrophic waters (Fig. 1). Initial surface chlorophyll *a* (Chl *a*) concentrations at these sites varied from 0.10 μg Chl *a* L^{-1} to 2.87 μg Chl *a* L^{-1}. Regions containing strong gradients were intentionally avoided when choosing experimental sites to minimize in situ changes due to advection. Surface-layer temperature and salinity characteristics of water parcels were assessed with MVP surveys to ensure coherency of water parcels over the duration of the experimental cycles.

Trophic cycling relationships—Our experiments provided rate estimates for phytoplankton growth and production, grazing processes, and export flux over the range of conditions sampled in the drogued water parcels. Growth and grazing measurements explained > 90% of the observed net rate of change in ambient phytoplankton chlorophyll (Landry et al. 2009); therefore, we formulate this net rate of change as the difference between biomass production and the combined grazing losses to micro- and mesozooplankton. We describe this relationship below in the format that is most commonly used in nutrient–phytoplankton–zooplankton models. Phytoplankton production (Eq. 1) is the product of biomass (P) and specific growth rate (μ_P, units of d^{-1}), and grazing losses are determined by the respective biomass-specific grazing rates (m_{SP} and m_{LP}, units of d^{-1} grazer biomass^{-1}) and biomasses (Z_S and Z_L) of micro- and mesozooplankton.

$$\frac{dP}{dt} = \mu_P \times P - m_{SP} \times Z_S \times P - m_{LP} \times Z_L \times P \qquad (1)$$

Accordingly, the combined terms $m_{SP}Z_S$ and $m_{LP}Z_L$ in Eq. 1 are the instantaneous grazing rates of the micro- and mesozooplankton assemblages, respectively, feeding on phytoplankton.

We assume that microzooplankton standing stock grows with a gross growth efficiency (GGE_1) of 30% (Straile 1997) and is grazed upon by mesozooplankton at the biomass-specific rate of m_{LZ}. Thus,

$$\frac{dZ_S}{dt} = \mathrm{GGE}_1 \times m_{SP} \times Z_S \times P - m_{LZ} \times Z_L \times Z_S \qquad (2)$$

Mesozooplankton likewise grow with a gross growth efficiency of GGE_2, yielding

$$\frac{dZ_L}{dt} = \mathrm{GGE}_2(m_{LP} \times Z_L \times P + m_{LZ} \times Z_L \times Z_S) \qquad (3)$$

As discussed further below, but consistent with the results of Landry et al. (2009), we assume that direct sinking of phytoplankton from the euphotic zone did not account for significant loss of biomass during our experiments. Fecal

matter produced by the feeding of mesozooplankton (F_{Prod}) can, therefore, be estimated from the trophic relationships described above, assuming an egestion efficiency (EE) of 30% (Conover 1966). If we further assume that the turnover time of fecal pellets with respect to sinking is fast relative to changes in the biotic community (*see* Discussion), then export can be approximated as

$$Export = F_{\text{Prod}} = \text{EE} \times (m_{LP} \times Z_L \times P + m_{LZ} \times Z_L \times Z_S) \quad (4)$$

Assuming steady-state conditions of microzooplankton standing stock over the few days of each experimental cycle, Eq. 2 simplifies to

$$\text{GGE}_1 \times m_{LP} \times Z_S \times P = m_{LZ} \times Z_L \times Z_S \quad (5)$$

and Eq. 4 becomes

$$Export = \text{EE} \times (m_{LP} \times Z_L \times P + \text{GGE}_1 \times m_{SP} \times Z_S \times P) \quad (6)$$

Dividing the entire equation by the gross growth rate of the phytoplankton community ($\mu_P P$), allows us to rewrite the equation in terms of the *e*-ratio:

$$e\text{-ratio} = \frac{\text{export}}{\mu_P P} = \text{EE} \times \left(\frac{m_{LP} Z_L}{\mu_P} + \frac{\text{GGE}_1 \times m_{SP} Z_S}{\mu_P} \right) \quad (7)$$

According to Eq. 7, the *e*-ratio, therefore, becomes a function of the egestion efficiency of mesozooplankton, the gross growth efficiency of the microzooplankton, and the ratios of micro- and mesozooplankton community grazing to phytoplankton-specific growth rate. While canonical values of 0.30 are used for both efficiency terms, the model results are relatively insensitive to ± 10% change in either of these parameters, due to the inherent variability in our repeated biological rate measurements (*see* Discussion).

An estimate of the *f*-ratio can be gleaned from our relationships if we assume that the rate of uptake of recycled nitrogen is equal to its rate of production. If we assume that phytoplankton do not exude nutrients and that C : N ratios are constant, the rate of production of recycled material is simply the difference between the gross phytoplankton growth rate ($\mu_P P$) and the rate of export and biomass accumulation (or depletion). Thus,

$$\text{Production of recycled nitrogen} = \mu_p P - F_{\text{Prod}} - \frac{dP}{dt} - \frac{dZ_L}{dt} \quad (8)$$

If we further assume that phytoplankton preferentially utilize available ammonium before nitrate, the total rate of recycled production becomes the minimum of Eq. 8 and total production (μ_PP). New production is the difference between total and recycled production; therefore, we can divide by total production ($\mu_P P$) to calculate an *f*-ratio:

$$f\text{-ratio} = \frac{\text{new}}{\text{total}} = \text{minimum}\left(0, e\text{-ratio} + \frac{dP/dt}{\mu_P P} + \frac{dZ_L/dt}{\mu_P P}\right) \quad (9)$$

By substituting in Eqs. 1, 3, and 7 and rearranging, we can see that the *f*-ratio is dependent on the rates of phytoplankton growth and micro- and mesozooplankton community grazing:

$$f\text{-ratio} = minimum\left(0, \frac{\mu_P - m_{SP} Z_S - m_{LP} Z_L}{\mu_P} + \frac{(\text{EE} + \text{GGE}_2)(m_{LP} Z_L + \text{GGE}_1 \times m_{SP} Z_S)}{\mu_P}\right) \quad (10)$$

This calculated *f*-ratio neglects nitrogen excretion by phytoplankton, which would decrease the ratio by a factor of 1 / (1 + % net primary production excreted). Given the uncertainties in our biological rate measurements, a relatively large excretion rate of 30% would still produce an *f*-ratio estimate within one standard error of the results of Eq. 10.

Biological rate parameters—As presented in Landry et al. (2009), daily instantaneous rates (d^{-1}) of phytoplankton growth (μ_p in our model) and microzooplankton community grazing (m_{comm}, equivalent to $m_{SP} Z_S$ in our model) were determined by two-point dilution experiments conducted in 2.7-liter bottle samples incubated at in situ temperature and light conditions on a line attached below our surface drifter. Eight sampling depths were chosen to span the euphotic zone, with the deepest bottle pair at a depth corresponding to roughly the 0.4% light level, which varied from 50 m inshore to 100 m offshore. The paired bottles represented whole (100%) seawater and 33% whole seawater, diluted with 0.1-μm filtered seawater. Water bottles were incubated for a 24-h period beginning and ending at ~ 04:00 h Pacific Standard Time each day. Rate assessments were based on initial and final 250-mL subsamples for Chl *a*. For consistency, all biological rates and standing stocks were vertically integrated to the depth of the deepest ^{14}C primary productivity (^{14}C-PP) incubation (35–40 m inshore and 70 m offshore).

Daily instantaneous rates of mesozooplankton community grazing on phytoplankton (M_{comm}, equivalent to $m_{LP} Z_L$ in our model) were determined from twice daily (midday and midnight) net tows using 202-μm mesh, 0.71-m diameter BONGO nets with attached flow meter towed to a maximum depth of 210 m (Landry et al. 2009; M. D. Ohman unpubl.). Daily community ingestion rates were calculated from the sum of the day–night means of Chl *a* and phaeopigment.

^{14}C-PP was measured in 4-liter samples incubated in polycarbonate bottles at six depths (Fig. 2A) on the in situ array. Triplicate 250-mL subsamples were filtered through GF/F filters, which were then fumed with HCl to remove inorganic ^{14}C. After addition of scintillation cocktail, beta decays were detected with a Beckman–Coulter scintillation counter.

^{234}Th-derived carbon export—^{234}Th deficiencies were calculated using a MnO_2 co-precipitation method (Benitez-Nelson et al. 2001; Buesseler et al. 2001; Pike et al. 2005). Samples (4-liter) were taken from eight depths per cast of a Niskin rosette (typically to a depth of approximately twice the euphotic zone). HNO_3 was added to the

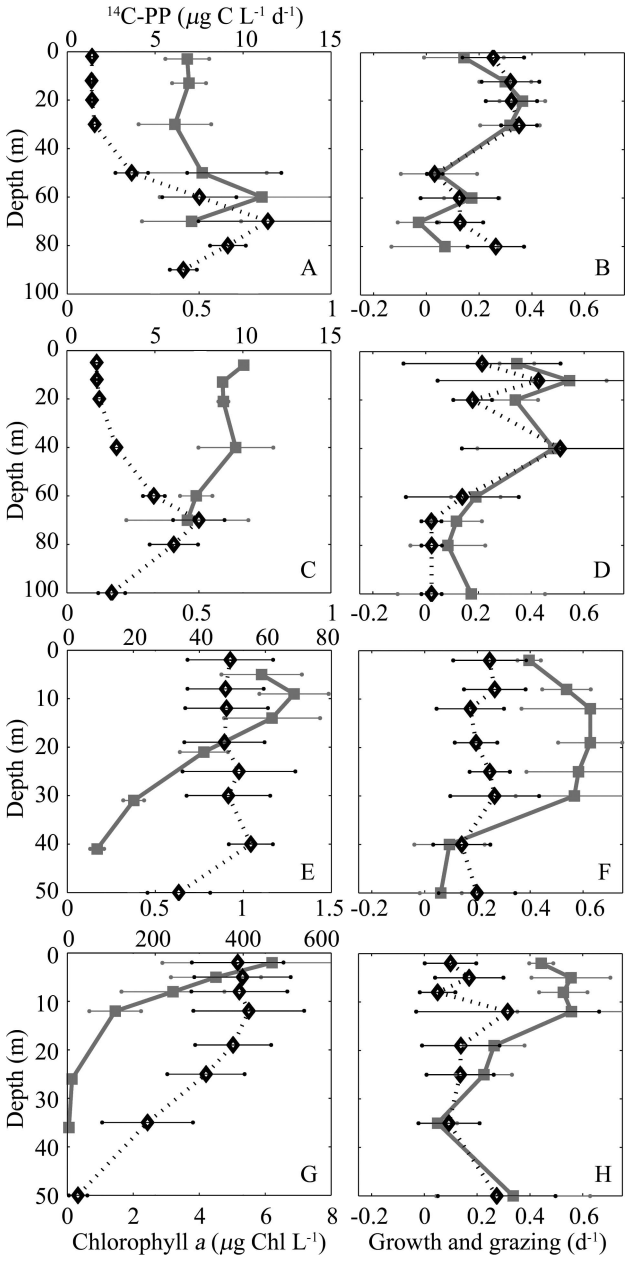

Fig. 2. Vertical profiles of chlorophyll, primary productivity, phytoplankton growth rate, and microzooplankton grazing rate. (A,B) Oligotrophic Offshore, (C,D) California Current Proper, (E,F) Inshore 2, and (G,H) Inshore 1. (A,C,E,G) squares and solid gray lines depict ^{14}C-PP, and diamonds with dotted lines are extracted Chl *a* concentrations. (B,D,F,H) squares and gray line are phytoplankton-specific growth rates from dilution experiments while diamonds and dashed lines are microzooplankton grazing rates. Error bars are ± one standard deviation of the repeat measurements taken over the course of the cycle.

samples to acidify to a pH of ~ 2, and the samples were immediately spiked with a known aliquot of ^{230}Th (1 mL at 0.17 Bq mL^{-1}) and allowed to sit for > 4 h. NH_4OH was then added to adjust pH to ~ 9, after which 100 μL each of 7.5 g L^{-1} $KMnO_4$ and 33 g L^{-1} $MnCl_2$ were added. Samples were shaken and let sit for > 8 h to allow Th to co-precipitate with MnO_2. The precipitates were vacuum-filtered onto a 25-mm quartz microfiber filter and allowed to air dry prior to mounting in a plastic holder (RISØ cup). They were counted on land with a low-level RISØ beta counter, followed > 6 half-lives later by a second count to establish background beta emission levels. To calculate the yield of the Th–MnO_2 co-precipitation, all samples were dissolved in 8 mol L^{-1} HNO_3 / 10% H_2O_2 solution and spiked with a gravimetrically measured aliquot of ^{229}Th (typically 1 g at 1.66 Bq g^{-1}). Samples were purified on a Poly-Prep chromatography column (Bio-Rad Laboratories) containing analytical grade anion exchange resin, chloride form (AG 1-X8 100–200, Bio-Rad Laboratories) and eluted with HCl. The HCl was subsequently evaporated off so that the residue could be reconstituted in a solution of 10% HNO_3/1% hydrofluoric acid for Inductively Coupled Plasma Mass Spectrometric Analysis of the ^{229}:^{230}Th-ratio at the Woods Hole Oceanographic Institution Analytical Lab. Recoveries averaged 80% ± 8% (mean ± SD). ^{234}Th deficiency was calculated as the difference between the measured activity and the expected activity if ^{234}Th was in equilibrium with ^{238}U, the latter being calculated from salinity as ^{238}U (mBq L^{-1}) = 1.143 × salinity × density (Chen et al. 1986). ^{234}Th export estimates for the three furthest offshore experimental cycles depicted in Fig. 1 were determined using a one-dimensional steady-state model [$E = \lambda_{Th}(A_U - A_{Th})$] and trapezoidal vertical integration, where E is vertical export, λ_{Th} is the decay constant of ^{234}Th, and A_U and A_{Th} are the activities of ^{238}U and ^{234}Th, respectively. While this steady-state approximation is an oversimplification of the complex cycling of particulate and dissolved thorium in the water column, it can provide a reasonable estimate of flux if ^{234}Th concentrations are near steady state and upwelling terms are negligible. It is the only feasible method of estimating carbon export from water parcels when repeat occupations over long (> 2-week) time periods are not possible. The potential errors associated with this steady-state approximation are addressed in our discussion.

Samples for particulate C : ^{234}Th-ratio were collected from beneath the euphotic zone, typically at 100 m (150 m for the furthest offshore cycle). A McLane large-volume water transfer system (WTS-LV) in situ pump was used to filter 200–300 liters of water through size-fractionated filters. We used a 75-μm prefilter to screen out swimming mesozooplankton that could significantly alter the measured C : ^{234}Th-ratio (Buesseler et al. 2006; Rodriguez Y Baena et al. 2006). Samples representative of sinking material were collected on 20-μm or 35-μm Nitex filters and then washed onto 25-mm quartz microfiber filters, which were dried and mounted on RISO cups for beta counting. Samples were beta-counted as with the ^{234}Th-deficiency samples, including a background count following decay of ^{234}Th. Samples were then combusted for carbon and nitrogen contents using a Costech 4010 Elemental combustion analyzer (Scripps Institution of Oceanography Analytical Laboratory).

Results

Comparison of measured and net rates—From the Lagrangian experimental approach, we measured trophic

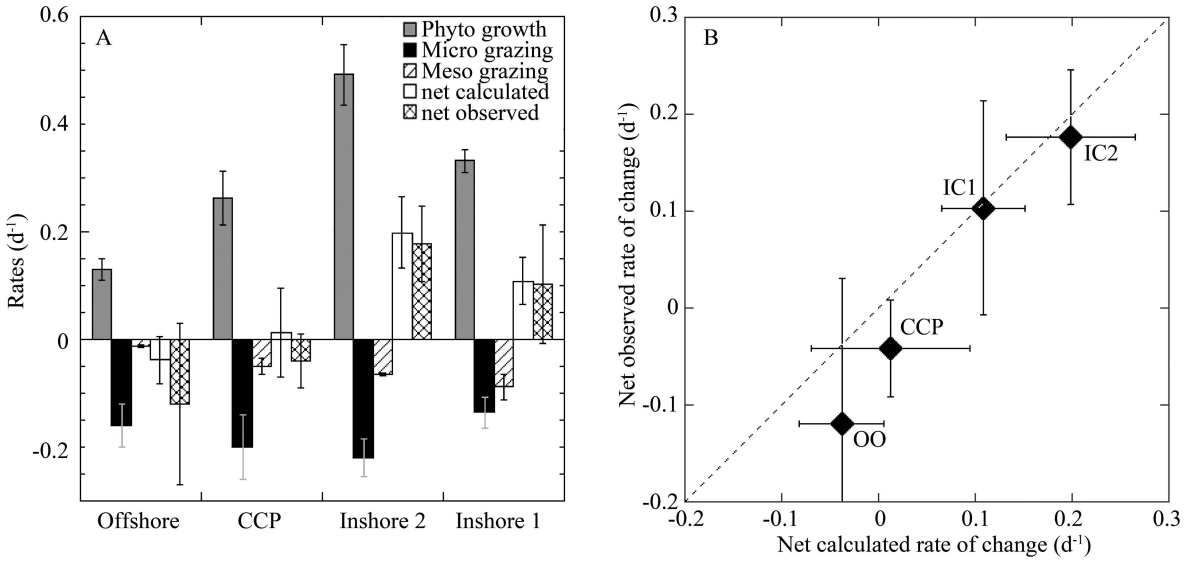

Fig. 3. Vertically integrated cycle averages. (A) Growth and grazing rates. Phytoplankton (Phyto) growth is the instantaneous growth rate as determined from Chl *a* analyses of our dilution treatments. Microzooplankton (Micro) grazing is determined from the dilution experiments. Mesozooplankton (Meso) grazing rates were measured from gut pigment measurements taken on oblique net tows. Net calculated growth rate is the difference between growth and grazing and matches well with the rates of change of chlorophyll measured over the course of each cycle as the water parcels evolved. Rates were vertically integrated to the depth of the deepest ^{14}C-PP incubation. The standard error of each measurement is shown. (B) Calculated and observed rate of change of the phytoplankton community. OO, CCP, IC1, and IC2 are the Offshore Oligotrophic, California Current Proper, Inshore 1, and Inshore 2 cycles, respectively.

process rates and carbon export in the CCE over conditions spanning a 30-fold range in mixed-layer chlorophyll. Microzooplankton grazing was the primary loss term for phytoplankton for all four cycles, accounting for 61% ± 15% to 92% ± 23% of the measured total grazing. Phytoplankton growth rates typically exceeded microzooplankton grazing pressure near the surface, but decreased more rapidly with depth relative to grazing rates (Fig. 2). This excess grazing over growth at depth likely consumed phytoplankton from the upper layer that either sunk slowly or were mixed deeper before they could be exported from the euphotic zone. ^{14}C-PP estimates of production were similar to the growth-based estimates derived from dilution experiments and microscopically determined phytoplankton biomass. Both patterns exhibited high surface productivity nearshore and a distinct subsurface maximum in productivity in the furthest offshore region.

Despite the relative constancy of microzooplankton grazing as a phytoplankton loss term, the percentage of phytoplankton growth consumed by microzooplankton differed appreciably in the experimental water parcels, varying from only 41% ± 9% inshore to 119% ± 34% of phytoplankton μ offshore. This stark difference drives the overall pattern in the calculated instantaneous net rates of phytoplankton growth ($\mu_P - m_{SP}Z_S - m_{LP}Z_L$), which varied from values of -0.04 ± 0.04 d^{-1} offshore to $+0.20 \pm 0.07$ d^{-1} inshore. Calculated net growth rates for the phytoplankton community were within the error of the net measured rates of change of chlorophyll in the euphotic zone calculated from daily Niskin rosette casts at the drifter locations (Fig. 3). The ability to predict reasonably well the in situ rate of change of the ambient community from process rate measurements using Chl *a* as a biomass proxy is a common feature of all four cycles. In the following three subsections, we present and contrast ^{234}Th export measurements and trophic cycling relationships in each of the three broad regions investigated: the oligotrophic offshore region, the California Current Proper, and the inshore region.

Offshore, oligotrophic water parcel (OOP)—Two of the water parcels studied are representative of the low-productivity waters found offshore in the CCE. The furthest offshore experiment was initiated 350 km from the coast in water far beyond the low-salinity core of the California Current, with the drogued parcel moving further seaward for the duration of our 4-d experimental cycle. Small cells dominated the phytoplankton community (A. G. Taylor pers. comm.), similar to conditions found throughout the subtropical Pacific (Venrick 1998, 2002). ^{234}Th profiles exhibit a strong subsurface maximum in deficiency, which corresponds to the depth of the subsurface production maximum measured by the ^{14}C-PP incubations. The particulate C : ^{234}Th sample (3.9 ± 0.5 mg C Bq^{-1}, mean ± measurement error) was collected on a 20-μm filter at a depth of 150 m to include flux out of the deep euphotic zone. Inspection of the ^{234}Th-deficiency profile shows that net remineralization probably began near 100 m. A comparison of the vertically integrated deficiencies between 100-m and 150-m (790 Bq m^{-2} and 675 Bq m^{-2}, respectively) suggests that as much as 15% of the ^{234}Th that sank out of the euphotic zone was remineralized before reaching the 150-m depth horizon, with likely a higher percentage of carbon remineralized, due

to preferential carbon remineralization (Buesseler et al. 2006). We calculated a ThE-ratio (ratio of ^{234}Th-derived carbon export to euphotic-zone–integrated ^{14}C-PP) of 0.15 ± 0.08 (mean ± SE, unless otherwise specified) for this water parcel.

The biological community for this experimental cycle was comprised of a small standing stock that exhibited relatively low mean growth rates for the euphotic zone, 0.13 ± 0.02 d^{-1}, and microzooplankton exceeded mesozooplankton grazing by an order of magnitude (Table 1). Measurements of combined grazing exceeded growth of the phytoplankton, leading to a slightly negative predicted net rate of change for the phytoplankton community, which closely matched the observed change in water-column chlorophyll concentrations (Fig. 3). Utilizing the measured community values for μ_p, $m_{SP}Z_S$, and $m_{LP}Z_L$, calculations from the trophic cycling model suggest an *e*-ratio of

$$e\text{-ratio} = \mathrm{EE} \times \left(\frac{m_{LP}Z_L}{\mu_P} + \mathrm{GGE}_1 \times \frac{m_{SP}Z_S}{\mu_P} \right)$$
$$= 0.3 \times \left(\frac{0.013}{0.13} + 0.3 \times \frac{0.16}{0.13} \right) = 0.14 \pm 0.03 \quad (11)$$

similar to the observed ThE-ratio of 0.15 ± 0.08.

California Current Proper (CCP) water parcel—The other experiment that sampled a water parcel characterized by relatively small phytoplankton cells, low chlorophyll concentration and low primary productivity was associated with the low-salinity core of the California Current. Our initial parcel for this experiment drifted into a restricted area after 2 d; so the experiment was reinitiated for another 2 d by moving to a location substantially upstream of the first. High shear below the mixed layer, combined with the complex vertical structure of the CCP (Lynn and Simpson 1987), likely led to advection of deeper water masses into our study site. This advection was probably responsible for the disparity between replicate ^{234}Th-deficiency profiles (Fig. 4B), particularly at depth. Vertically integrated deficiency (integrated to 100 m = 603 ± 185 Bq m^{-2}) and C : ^{234}Th-ratio (100 m, 35-μm filter, 4.2 ± 0.5 mg C Bq^{-1}, mean ± measurement error) were similar to those found in the OOP cycle, but the higher rates of primary productivity led to a slightly lower ThE-ratio of 0.12 ± 0.04.

The phytoplankton community of the CCP was largely at steady state during the time of our sampling, with a net growth rate of −0.04 ± 0.05 d^{-1}. Chlorophyll concentrations were comparable to that of the oligotrophic offshore water, but specific growth rates were significantly higher and balanced by losses to grazing, dominated by microzooplankton, but with mesozooplankton accounting for a substantial (> 20%) portion. Our trophic cycling model predicted an *e*-ratio of 0.13 ± 0.03, which was close to the measured ThE-ratio.

Inshore water parcels—The two water parcels studied inshore of the CCP were dominated by larger phytoplankton (A. G. Taylor pers. comm.) and had higher chlorophyll concentrations characteristic of the coastal area affected by

Table 1. Vertically integrated ecosystem values. 'μ_P' is the specific growth rate of the phytoplankton (d^{-1}). '$m_{SP}Z_S$' is the specific grazing rate of the microzooplankton community (d^{-1}). '$m_{LP}Z_L$' is the specific grazing rate of the mesozooplankton community (d^{-1}). '$\mu - m_{SP}Z_S - m_{LP}Z_L$' is the calculated net growth rate of the phytoplankton (d^{-1}). 'Net obs' is the observed net growth rate of the ambient phytoplankton community (d^{-1}). 'PP' is ^{14}C-derived primary productivity (mg C m^{-2} d^{-1}). '^{234}Th Export' is the vertical flux of ^{234}Th across the 100-m (150-m for the offshore cycle) depth horizon (Bq m^{-2} d^{-1}) as calculated with a one-dimensional steady-state model. 'C : Th' is the carbon : ^{234}Th-ratio collected from beneath the euphotic zone (mg C Bq^{-1}) with a large volume (200–300 liters) in situ pump. 'Export' is carbon export calculated with a one-dimensional steady-state model (mg C m^{-2} d^{-1}). 'ThE' is the ratio of export to primary productivity. 'Trophic *e*' is the *e*-ratio determined from our trophic relationships. All biological parameters were integrated to the depth of the deepest primary productivity incubation and averaged over the length of the cycle, while ^{234}Th parameters were integrated down to 100 m (150 m for the offshore cycle) and averaged over the cycle duration. Values are mean ± standard error of the repeat measurements for all measurements except C : Th-ratio, which reports mean ± error associated with carbon and ^{234}Th measurements.

Cycle	μ_P (d^{-1})	$m_{SP}Z_S$ (d^{-1})	$m_{LP}Z_L$ (d^{-1})	$\mu_P - m_{SP}Z_S - m_{LP}Z_L$ (d^{-1})	Net obs (d^{-1})	PP (mg C m^{-2} d^{-1})	^{234}Th Export (Bq m^{-2} d^{-1})	C : Th (mg C Bq^{-1})	C Export (mg C m^{-2} d^{-1})	ThE	Trophic *e*
Offshore	0.13±0.02	0.16±0.04	0.013±0.002	−0.04±0.04	−0.12±0.15	520±100	19.5±9.3	3.9±0.5	76±38	0.15±0.08	0.14±0.03
CCP	0.26±005	0.20±0.06	0.050±0.015	0.01±0.08	−0.04±0.05	610±10	17.3±5.3	4.2±0.5	72±23	0.12±0.04	0.13±0.03
Inshore 1	0.33±0.02	0.14±0.03	0.088±0.024	0.11±0.04	0.10±0.11	4940±830	15.3±2.8	—	—	—	0.12±0.02
Inshore 2a	0.48±0.08	0.21±0.05	0.066±0.006	0.20±0.09	0.14±0.09	1760±160	19.0±1.0	8.0±1.0	151±15	0.09±0.01	0.08±0.01
Inshore 2b	0.54±0.14	0.24±0.11	0.064±0.023	0.23±0.18	0.28±0.53	1420±330	31.3±9.3	3.0±0.3	94±30	0.07±0.03	0.08±0.03

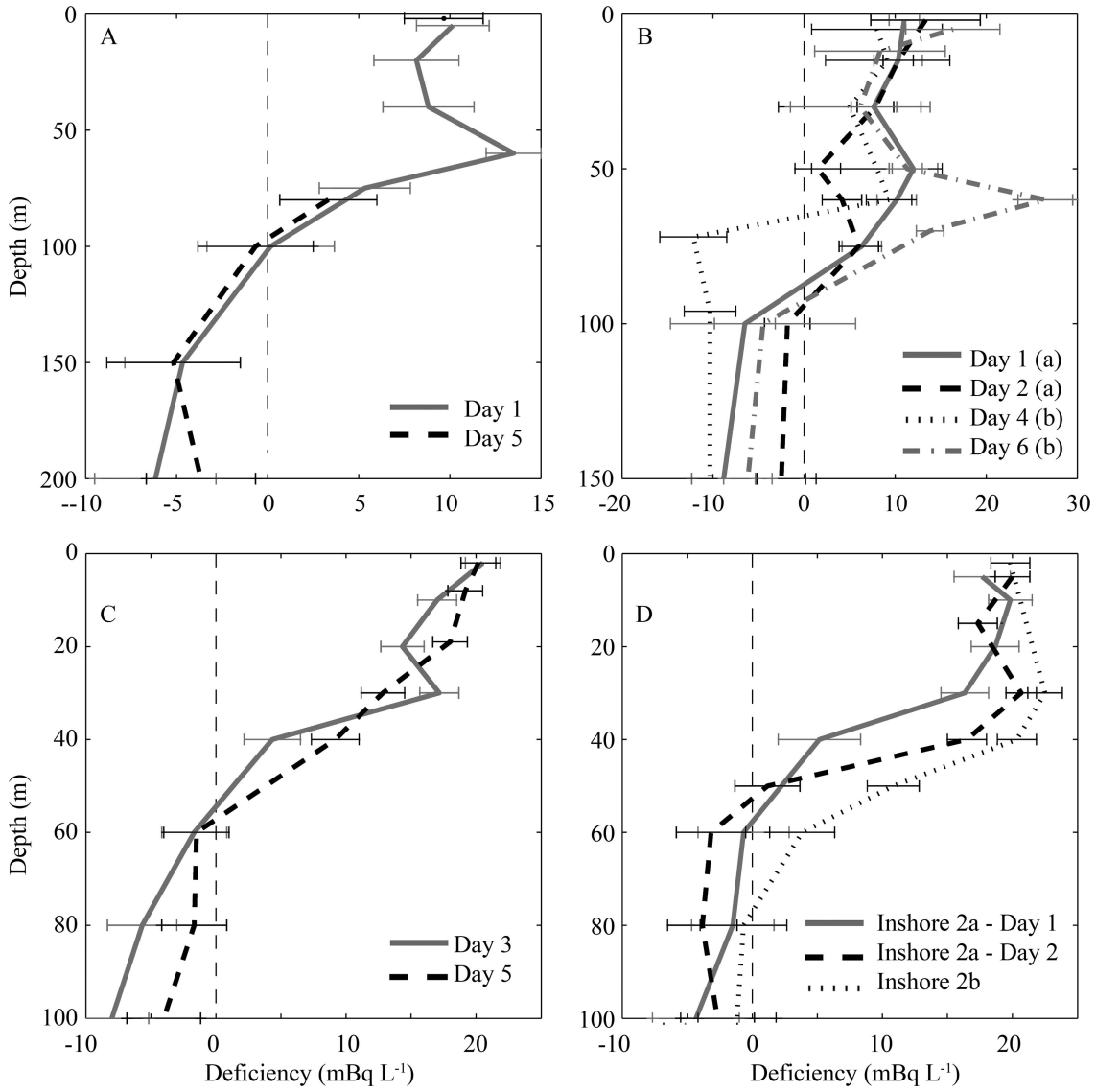

Fig. 4. ^{234}Th deficiency in (A) Oligotrophic Offshore, (B) California Current Proper, (C) Inshore 1, and (D) Inshore 2 water parcels. Error bars were determined by propagating errors from volume measurements, counting statistics, and the errors in yield calibrations. When yield analyses were not possible (because samples were lost during column chromatography), yield was assumed to be the average yield (80%) of each individual measurement with a larger error derived from the standard deviation of the yield measurements.

seasonally variable upwelling (Venrick 1998, 2002). The cold temperatures and high salinities of these parcels are indicative of recently upwelled water, and we believe they had similar origins near Point Conception. Our sampling for inshore Cycle 1 (IC1) began roughly 30 km off the coast, and the drifter tracked almost directly offshore (west) for 4 d, with an average velocity of 11 km d^{-1}. Inshore Cycle 2 (IC2) began 15 d later 80 km from the coast and also drifted west at an even higher speed. The drifter was lost after providing 3 d of data (IC2a), but a new experiment was initiated close to where the first drifter was lost to obtain an additional day of rate measurements (IC2b). Similar histories of Inshore Cycles 1 and 2 are suggested by mixed-layer temperature–salinity profiles, which showed similar trajectories of warming and freshening as the water parcels advected offshore; in fact, the continued evolution of IC1 might have resulted in conditions similar to the physical parameters observed at the start of IC2. While IC1 still retained significant concentrations of upwelled nitrate in the euphotic zone (initial surface concentrations > 13 μmol L^{-1}, decreasing with time), IC2 was depleted in nitrate at the surface (< 1 μmol L^{-1}) with a strong nitracline near 40 m.

The simple steady-state model predicts a ^{234}Th export rate of 15.5 $\pm$ 2.8 Bq m^{-2} d^{-1} for IC1. However, the dynamic nature of this region led us to question the applicability of the steady-state assumption. A complete mass-balance model of ^{234}Th for IC1 should involve both a non–steady-state term and terms for horizontal and vertical advection and diffusion (Savoye et al. 2006):

$$\frac{\partial A_{Th}}{\partial t} = \lambda_{Th}(A_U - A_{Th}) - E + V \quad (12)$$

where, as before, A_U and A_{Th} are the activities of ^{238}U and ^{234}Th, respectively, λ_{Th} is the decay constant of ^{234}Th, E is the export of ^{234}Th on vertically sinking particles, and V is the sum of vertical and horizontal advective and diffusive water movements. Although we can tentatively neglect horizontal advection due to our Lagrangian sampling strategy, non–steady-state effects associated with recent upwelling may be significant, though mesoscale wind conditions suggested that our cruise coincided with a period of relaxation of upwelling (Rykaczewski and Checkley 2008). Assuming a typical upwelling rate of 1 m d^{-1} prior to our occupation of IC1 and the vertical ^{234}Th gradient of 0.25 mBq L^{-1} m^{-1}, we calculate that an additional 25 Bq m^{-2} d^{-1} would be added to the $^{234}Th:^{238}U$ deficiency export term of 15.3 ± 2.8 Bq m^{-2} d^{-1}. Thus, the total export of ^{234}Th for this upwelling affected cycle may be > 150% higher than that derived from the steady-state assumption. Unfortunately, a technical failure prevented us from measuring the $C:^{234}Th$-ratio of exported particulates for this cycle; hence, we cannot reliably convert the ^{234}Th export measurement to its C export equivalent.

IC2 is a better fit to the assumptions required for steady state. A slightly decreasing surface-water density, combined with the aforementioned wind measurements, suggest that upwelling was not significant at this time. A comparison of the vertically integrated deficiencies for the final day of IC1 (632 Bq m^{-2}) and the first day of IC2 (625 Bq m^{-2}) further indicates that the inclusion of a non–steady-state term would have negligible impact on the export calculation (*see* Discussion). Repeat profiles also suggest that differences within IC2a were due to a deepening of the thermocline and nitracline from 38 m to 42 m, perhaps driven by some combination of downwelling and/or internal waves and tides. Further support for a steady-state interpretation comes from the rapid switch from net deficiency to net remineralization at the base of the (~ 50-m) euphotic zone for IC2a. IC2b (a separate 1-d experiment) was in a slightly different water mass that showed a higher deficiency (1090 ± 330 Bq m^{-2} vs. 662 ± 37 Bq m^{-2} for IC2b and IC2a, respectively) and lower $C:^{234}Th$-ratio (3.0 ± 0.1 mg C Bq^{-1} vs. 8.0 ± 1.0 mg C Bq^{-1} and for IC2b and IC2a, respectively). We, therefore, use separate $C:^{234}Th$-ratios for the two segments of IC2 to calculate carbon export across the 100-m depth horizon.

Although IC1 had a significantly higher biomass than IC2, the biological community behaved similarly in both inshore cycles. For both cycles (including both sections of IC2), growth exceeded grazing, and the ambient phytoplankton grew at net rates similar to those predicted experimentally (Fig. 2; Table 1). Mesozooplankton grazing was slightly higher during IC1 than IC2, contributing 39% ± 29% of grazing compared to 23% ± 25%. Our trophic relationships suggested an *e*-ratio of 0.08 ± 0.01 for IC2a compared to a ThE-ratio of 0.09 ± 0.01, and an *e*-ratio of 0.08 ± 0.03 compared to a ThE of 0.07 ± 0.03 for IC2b. For IC1, the trophic relationships predicted an *e*-ratio of 0.12 ± 0.02, but, as mentioned previously, the lack of a $C:^{234}Th$-ratio did not allow us to calculate a corresponding ThE-ratio.

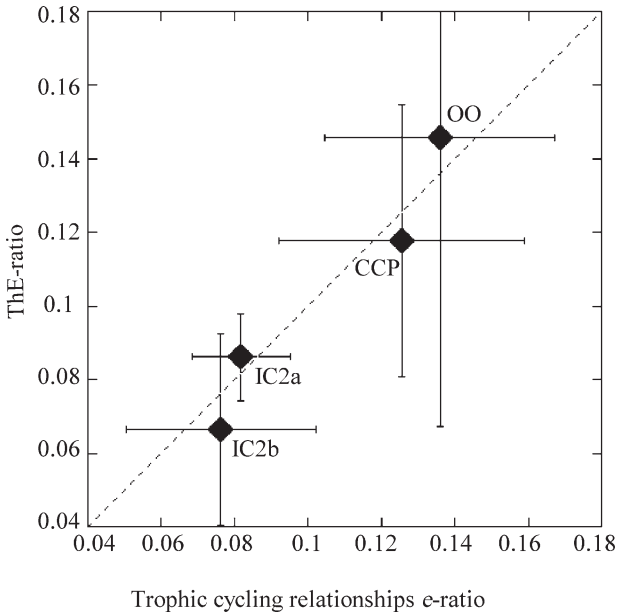

Fig. 5. Comparison of trophic cycling relationships to ^{234}Th-deficiency steady-state model. OO, CCP, IC2a, and IC2b are the Offshore Oligotrophic, California Current Proper, Inshore 2a, and Inshore 2b cycles, respectively.

Discussion

Trophic cycling and carbon export—In this study, a suite of measurements allows us to assess biological regulation of two biogeochemically relevant processes, autotrophic biomass accumulation and vertical carbon flux. By making process rate measurements while monitoring the temporal evolution of the phytoplankton community, Landry et al. (2009) demonstrated that phytoplankton growth and grazing losses determine to first order the observed net growth rates of the phytoplankton in the CCE. We confirm these results via the strong correlation between calculated and observed net rates of change (Fig. 3B). The slight average overestimate (0.04 d^{-1}) in the calculated vs. observed rates of change reflects, in part, our choice (for consistency) to integrate all rates only to the depth of the deepest primary productivity sample incubations. Growth typically decreases more rapidly with depth than grazing (Landry et al. 2011); therefore, our grazing loss estimates are conservative.

Our simple trophic model builds on these previous findings to explain the variability of *e*-ratios (hence, vertical carbon flux) determined in May 2006 (Fig. 5). In fact, ^{234}Th steady-state estimates of export are in good agreement with those predicted from measured growth and grazing rates and the trophic model, and are well within margins of error for all cycles for which carbon export could be assessed (Cycles 2–4). This agreement, despite major differences in the planktonic communities investigated, suggests that the underlying processes regu-

lating export are relatively similar throughout the system. While net phytoplankton growth rate is highly variable and driven by the balance between growth and grazing processes dominated by microzooplankton, export rates are consistent with the sum of direct and indirect trophic linkages between phytoplankton and mesozooplankton.

It is important to note that the rates used for *e*-ratio calculations (specific growth, micro- and mesozooplankton grazing; all using Chl *a* as a biomass indicator) were entirely distinct from the measurements used to calculate ThE-ratios (^{234}Th deficiency, C : ^{234}Th-ratio, ^{14}C-PP). Furthermore, the independent parameters in the calculations (egestion efficiency and GGE) were not tuned to the data; we used canonical mean values of 0.30 for both. Thus, the ability to explain the generally low magnitude and two-fold variability in ThE-ratio is a striking result, suggesting that we may have reasonably represented the processes that regulate carbon export in this system. At worst, it indicates that the Th-derived export estimates are consistent with reasonable inferences about the plankton trophic interactions leading to fecal-pellet production by mesozooplankton.

Export measurements—Unlike sediment traps, which measure export from a statistical funnel above the trap (Siegel et al. 1990), radionuclide disequilibria estimate export from specific patches of water, thus fitting the spatial scale of our contemporaneous ecological measurements. Interpreting deficiency profiles requires understanding of, or assumptions about, advection and diffusion effects on the radionuclide budget, as well as non–steady-state processes associated with episodic export (*see* Eq. 12). Diffusive fluxes are typically neglected assuming that horizontal gradients and vertical diffusivity are both minimal. For our Lagrangian sampling plan, we also neglected horizontal advection, and mesoscale wind measurements during our cruise indicated that upwelling was minimal (Rykaczewski and Checkley 2008: fig. 2).

The assumption of temporal steady state is nonetheless a major issue, particularly at inshore sites where high springtime productivity and biomass accumulation can lead to episodic export events. Ideally, we should track water parcels for $>$ 1 week (Savoye et al. 2006) to measure the temporal evolution of water-column deficiencies accurately. However, truly effective tracking is difficult, at best, and more likely impossible, in regions with vertical shear and horizontal heterogeneity. IC2a seems to have sampled similar water to IC1 that aged as it moved offshore; therefore, we can use these cycles to begin to address the potential role of the non–steady-state term, dA_{Th}/dt in Eq. 12. From the mean deficiencies for IC1 and IC2a (530 $\pm$ 100 Bq m^{-2} and 662 $\pm$ 37 Bq m^{-2}, respectively) and the time difference between the ^{234}Th measurements (12.7 d), we calculate a NSS export of 29.8 $\pm$ 8.1 Bq m^{-2} d^{-1} (mean $\pm$ SE) for the period between the two cycles. By this calculation, the steady-state export estimate of 19.0 $\pm$ 1.2 Bq m^{-2} d^{-1} for IC2a may be low by $\sim$ 36%, but 95% confidence intervals for the two determinations are not statistically different. However, because we have no way of confirming that IC2 was aged IC1 water, the magnitude of the NSS export correction remains uncertain.

Table 2. Calculated, vertically integrated estimates of *f*-ratios. $f_{Harrison}$ uses ambient NO_3 and NH_4 concentrations, ^{14}C-PP, and the *f*-ratio relationship developed by Harrison et al. (1987): *f*-ratio = m $\times$ (NO_3 / (NO_3 + NH_4)) + b, with m = 0.77 $\pm$ 0.10, b = 0.06 $\pm$ 0.02 (representative of the Southern California Bight). $f_{trophic}$ is calculated from our trophic relationships. For $f_{Harrison}$, errors include standard error of repeat measurements, as well as the uncertainty in parameters m and b. Error on $f_{trophic}$ is propagation of standard errors from repeat measurements. For the offshore cycle, the model predicted that ammonium production slightly exceeded total phytoplankton production (by 1%), but with a standard error that suggested the *f*-ratio may have been as high as 0.36.

	$f_{Harrison}$	$f_{trophic}$
Offshore	0.34$\pm$0.13	0(0–0.36)
CCP	0.31$\pm$0.08	0.30$\pm$0.31
Inshore 1	0.79$\pm$0.27	0.56$\pm$0.13
Inshore 2	0.57$\pm$0.11	0.58$\pm$0.10

Decoupling of new and export production—With typical *f*-ratios ranging from 0.2 to 0.8 in the Southern California Bight (Eppley et al. 1979), new production generally exceeds export production inshore of the CCP (Nelson et al. 1987). Based on the Eppley et al. (1979) measurements, Harrison et al. (1987) found a linear relationship (slope = 0.77 $\pm$ 0.10; intercept = 0.06 $\pm$ 0.02) between new production and the nutrient ratio of [NO_3^-] / ([NO_3^-] + [NH_4^+]). We calculated *f*-ratios from the Harrison et al. (1987) equations at each of our ^{14}C-PP sampling depths and vertically integrated and averaged these over the euphotic zone. The results agree closely with trophic calculations based on Eq. 10 (Table 2), both predicting *f*-ratios of 0.6 to 0.8 for the nearshore cycles and $\sim$ 0.3 for the CCP. For the OOP cycle, the trophic cycling equations predict no new production, while the $NO_3 : NH_4^+$ ratio indicates an *f*-ratio of 0.34. This discrepancy could have resulted from nutrient measurement inaccuracies at low concentrations. Nevertheless, both calculations clearly predict significantly higher *f*-ratios inshore, relative to the low measured and modeled *e*-ratios in this region.

Olivieri and Chavez (2000) and Plattner et al. (2005) hypothesized that offshore transport of upwelled water near the California coast led to spatiotemporal decoupling of new and export production. The obvious disparity between our *e*- and *f*-ratios (Fig. 6) supports this view, and our Lagrangian sampling offers a unique perspective on the underlying processes. All of our inshore water parcels drifted rapidly offshore (net speeds of 13 cm s^{-1}, 20 cm s^{-1}, and 18 cm s^{-1} for IC1, IC2a, and IC2b, respectively) while we measured net positive growth rates for the phytoplankton. Particulate organic carbon and chlorophyll also accumulated during offshore transport, with mean net rates of chlorophyll increase of 0.10 d^{-1}, 0.14 d^{-1}, and 0.28 d^{-1} for IC1, IC2a, and IC2b, respectively.

Assumptions, sensitivity, and the protozoan food web—We used fixed canonical values for GGE and EE model

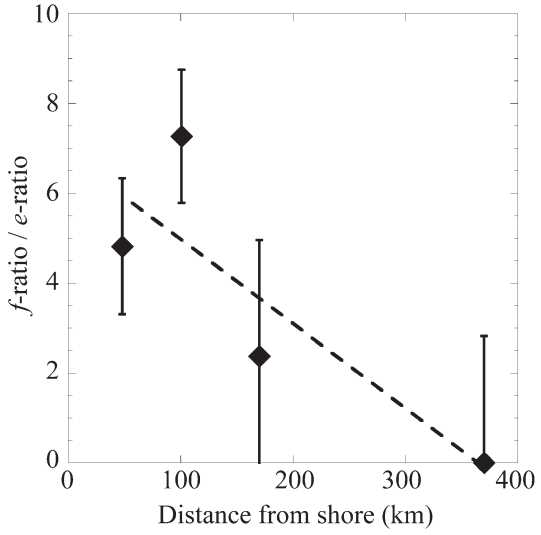

Fig. 6. Decoupling of export and new production. y-axis is the trophic cycling *f*-ratio divided by *e*-ratio. x-axis is distance from shore of each cycle (km). Error bars are ± standard error. Dashed line is a linear regression: y = 6.9 − 0.019x, R^2 = 0.72.

parameters, although actual efficiencies for in situ communities are uncertain and likely variable. The effects of uncertainty in these assumed efficiencies on modeled export and new production rates can be determined by differentiating Eqs. 7 and 10 with respect to GGE or EE. While a percentage decrease in EE yields a proportional decrease in modeled export, the response of the e-ratio to varying protozoan GGE depends on the ratio of protozoan : mesozooplankton grazing, but will always be less than a comparable change in EE. A change in either EE or GGE for mesozooplankton leads to an *f*-ratio change proportional to the ratio of total mesozooplankton ingestion to phytoplankton growth:

$$\frac{\mathrm{d}f\text{-ratio}}{d\mathrm{EE}} = \frac{\mathrm{d}f\text{-ratio}}{d\mathrm{GGE}_2} = \frac{m_{LP}Z_L + \mathrm{GGE}_1 \times m_{SP}Z_S}{\mu_P} \quad (13)$$

With reasonable inferences, we can also assess the impact of key assumptions dealing with zooplankton and fecal-pellet steady-state conditions and the number of protistan trophic levels. If we assume that protozoan biomass is roughly half of phytoplankton biomass, we can solve eq. 4 with different percent rates of change of the protozoan biomass to assess the effect of our steady-state microzooplankton assumption on the *e*-ratio. With this assumption, a 10% d^{-1} increase in microzooplankton standing stock decreases the *e*-ratio by 0.05. The agreement between our ^{234}Th measurements and trophic cycling relationships implies that microzooplankton were near steady state. Nonetheless, the relatively high sensitivity of the e-ratio result to protistan biomass variations highlights the importance of accurate measurements of the protozoan community. While our trophic cycling relationships included no closure term (implicitly assuming that mesozooplankton biomass accumulated during the spring upwelling period), the alternative is for mesozooplankton to be cropped by larger carnivores:

$$\frac{dZ_n}{dt} = \mathrm{GGE_n} \times m_{n,n-1} \times Z_n \times Z_{n-1} - m_{n+1,n} \times Z_{n+1} \times Z_n = 0 \quad (14)$$

where Z_n is the biomass of trophic level n and $m_{n,n-1}$ is the grazing of the trophic level n on trophic level $n-1$. Solving Eq. 14 shows that the grazing rate of any trophic level will be equal to the product of the lower trophic level's grazing rate and GGE. Thus, assuming constant GGE and EE, fecal-pellet production decreases by the GGE for each trophic-level increase. An upper limit for the effect of increased fecal-pellet production by mesozooplankton is, thus, the sum of an infinite geometric series ($\Sigma\mathrm{GGE^n} = 1 / [1 - \mathrm{GGE}]$), which increases total export by a factor of 1.43 for GGE = 0.3 at all levels. Although this alternate assumption allows us to derive an upper-limit estimate for the potential contribution of higher trophic levels to vertical carbon flux, we caution that mesozooplankton with long turnover times should not be expected to be in local steady-state in an advective environment (Gruber et al. 2006). The effect of our assumption that fecal-pellet concentrations are at steady-state (or alternately, that they sink infinitely fast) cannot be tested because we lack estimates of fecal-pellet concentrations and turnover times. However, typical small crustacean fecal-pellet sinking rates of 20–100 m d^{-1} (Turner 2002) suggest only slight decoupling of fecal-pellet production and export during our 4-d cycles.

Our rate relationships for the CCE imply an important shunt of production from phytoplankton via microzooplankton to mesozooplankton, with a single trophic step on average. However, traditional formulations of the microbial loop (Azam et al. 1983) assume multiple trophic transfers within the protozoa and, hence, higher remineralization. To allow for an additional number of trophic transfers among protists, we need only add an exponent, *n,* to the microzooplankton GGE, which represents the average number of trophic steps that separate phytoplankton from mesozooplankton:

$$e\text{-ratio} = \mathrm{EE} \times \left(\frac{m_{LP}Z_L}{\mu_P} + \mathrm{GGE^n} \times \frac{m_{SP}Z_S}{\mu_P} \right) \quad (15)$$

The need to vary this parameter would obviously be greater in biological communities dominated by very small phytoplankton and with high grazing impact of microzooplankton, as is generally the case in the open ocean (Calbet and Landry 2004). Although our coastal–offshore differences in microzooplankton grazing (42–44% vs. 77–123%, respectively) were more extreme than the global averages (60% coastal, 70% oceanic; Landry and Calbet 2004), there was adequate food chain transfer for the OOP to support a moderate rate of export via mesozooplankton, in fact the highest *e*-ratio that we measured. Thus, the efficiency of transfer from micro- to mesozooplankton becomes an important determinant of the amount of primary productivity that can be exported. If we assume only a single trophic step within the microzooplankton in our experiments, then the relative proportion of mesozooplankton nutrition

derived from microzooplankton ranges from 32% to 79% for our four cycles, which agrees well with the percent carnivory suggested by the C : phaeopigment measurements of Small and Ellis (1992). Our relationships, therefore, indicate that, far from being strictly a remineralization pathway, the microzooplankton in the CCE shunt a significant amount of carbon into export.

Time scales and the export ratio—Our measurements show an inverse relationship between primary productivity and export efficiency in the CCE region during springtime, which runs contrary to the predictions of two mechanistic models of the biological control of carbon export (Laws et al. 2000; Dunne et al. 2005). Because they are developed for different spatial and temporal scales, the Laws et al. (2000) and Dunne et al. (2005) models reasonably predict broad global patterns in export, but fail to predict intra-regional export patterns, as seen in the present study, the Southern Ocean (C. D. Nevison unpubl.), and in several low-productivity regions (Dunne et al. 2005). Additionally, while our trophic relationships and experimental design explicitly account for biomass accumulation and decoupling of new and export production, the steady-state models of Laws et al. (2000) and Dunne et al. (2005) assume both a spatial and temporal equality between new and export production. Given this assumption, it is worth noting that the emergent result of these two steady-state models, namely the positive correlation between phytoplankton biomass and *e*-ratio, may have arisen from two independent ecological relationships: The input of new nitrogen stimulates phytoplankton growth (particularly large phytoplankton), leading to a correlation between *f*-ratio and primary production (Eppley and Peterson 1979). Meanwhile, large phytoplankton have higher individual sinking rates (Smayda 1970) and shorter pathways to higher trophic levels (Michaels and Silver 1988), thus potentially leading to higher *e*-ratios. Although steady-state models cannot differentiate between these two mechanisms, our results suggest that the *ef*-ratio in these models may reflect new production, rather than export.

Nevertheless, our trophic cycling relationships, which explicitly assume that phytoplankton are not at steady state, do not indicate an inverse relationship between phytoplankton size and export efficiency. Given the higher ratio of mesozooplankton : protozoan grazing in the productive nearshore waters, our model suggests a positive relationship between primary production and export efficiency if the system is in steady state. However, during the temporally dynamic period of our study, the strongest pattern that emerged was an inverse relationship between net growth rate of the phytoplankton community and export efficiency. In the OOP cycle, phytoplankton biomass declined over 4 d, and we measured a relatively high ThE-ratio. Conversely, in the inshore region of accumulating phytoplankton biomass, the ThE-ratio was lower. Over longer time periods than the experimental cycles, we would expect phytoplankton to reach a quasi–steady state, with growth balanced by grazing and other loss processes. Mechanistically, it looked like zooplankton grazing had temporarily outpaced phytoplankton growth in the offshore experimental site and, hence, was reducing community biomass and primary production. Reduced food resources for protozoan grazers and, perhaps, mesozooplankton switching predation pressure from phytoplankton to microzooplankton, would presumably resolve this imbalance in time, allowing phytoplankton to increase. Nutrient decline and increasing grazing capacity would serve similarly as negative feedbacks to bring the accumulating phytoplankton biomass in the inshore area back into balance.

These patterns suggest a system in which contemporaneous imbalances of growth and grazing lead to autotrophic biomass accumulation (rather than sinking out of the euphotic) or net heterotrophy on short time scales, while export measurements and the drivers of export reflect longer (weekly) time scales. The failure of steady-state mechanistic models to predict intra-regional patterns in export efficiency further suggests that such models may have limited ability for predicting ecosystem shifts in response to changing climate. Within the CCE region, vertical carbon export seems to be reasonably explained by food-web processes leading to mesozooplankton consumption and fecal-pellet production. The central role of zooplankton as mediators of carbon flux in this model suggests a potential coupling between climate-associated community changes and carbon export in the CCE. The secular warming trend evident in CalCOFI data (Roemmich 1992) has been linked, for example, to a 70% decline in the biovolume of large zooplankton (Roemmich and McGowan 1995), notably a decrease in salps (Lavaniegos and Ohman 2007). It is tempting to infer from this that export pathways may also have diminished. However, extrapolating from short-term studies to longer time scales is problematic, because export fluxes due to sinking phytoplankton and/or subduction of particulate and dissolved organic carbon may also have undergone compensatory changes in time or space.

In summary, we found that calculations based on simple trophic relationships and experimental rate measurements in the CCE were consistent with measured variations in the *e*-ratios of water parcels representing a range of conditions from recently upwelled coastal water to oligotrophic offshore regions. The good agreement between independently measured ecological and biogeochemical rates in these very different plankton assemblages suggest that zooplankton dynamics are a primary driver of vertical carbon flux in this system. For the range of conditions studied, variability in export efficiency was determined by the local net balance of growth and grazing processes and the relative strengths of grazing pathways through microzooplankton vs. directly to mesozooplankton. This study was limited, however, to a few water parcels, representative, at best, of the region during springtime. Therefore, further work is necessary to assess biological controls of carbon export under different seasonal conditions, as well as to quantify and compare results to purely physical mechanisms of export, such as subduction fronts. In this regard, the Lagrangian design that we used to obtain the rate measurements for this study appears to be a workable approach for constraining ecological and biogeochemical

relationships in complex coastal regions, with the eventual goal of extending these relationships into mechanistic models with predictive power.

Acknowledgments

We thank the captain and crew of the R/V *Knorr* for their professionalism and contributions to conducting these experiments at sea. We are grateful to all of our colleagues in the California Current Ecosystem, Long-Term Ecological Research (CCE LTER) program for their support and collaboration, and particularly to M. D. Ohman for providing the mesozooplankton grazing results. We give special thanks to M. Décima, S. Dovel, M. Roadman, R. Rykaczewski, J. Powell, D. Taniguchi, and K. Tsyrklevich for their assistance at sea and in laboratory analyses, and to M. D. Ohman, P. J. S. Franks, and two anonymous reviewers for insightful comments and suggestions.

This work was supported by National Science Foundation (NSF) funding (Ocean Sciences grant 04-17616) for the CCE LTER site, and by graduate research fellowships (NSF and National Aeronautics and Space Administration Earth and Space Science) to M. Stukel.

References

Alldredge, A. L., and C. C. Gotschalk. 1989. Direct observations of the mass flocculation of diatom blooms: Characteristics, settling velocities and formation of diatom aggregates. Deep-Sea Res. **36:** 159–171.

Armstrong, R. A., C. Lee, J. I. Hedges, S. Honjo, and S. G. Wakeham. 2002. A new, mechanistic model for organic carbon fluxes in the ocean based on the quantitative association of POC with ballast minerals. Deep-Sea Res. Part II **49:** 219–236, doi:10.1016/S0967-0645(01)00101-1

Azam, F., T. Fenchel, J. G. Field, J. S. Gray, L. A. Meyer-Reil, and F. Thingstad. 1983. The ecological role of water-column microbes in the sea. Mar. Ecol. Prog. Ser. **10:** 257–263, doi:10.3354/meps010257

Benitez-Nelson, C. R., K. O. Buesseler, M. R. Van Der Loeff, J. Andrews, L. Ball, G. Crossin, and M. A. Charette. 2001. Testing a new small-volume technique for determining Th-234 in seawater. J. Radioanal. Nucl. Chem. **248:** 795–799, doi:10.1023/A:1010621618652

Buesseler, K. O. 1998. The decoupling of production and particulate export in the surface ocean. Glob. Biogeochem. Cycles **12:** 297–310, doi:10.1029/97GB03366

———, M. P. Bacon, J. K. Cochran, and H. D. Livingston. 1992. Carbon and nitrogen export during the JGOFS North Atlantic Bloom Experiment estimated from $^{234}Th:^{238}U$ disequilibria. Deep-Sea Res. **39:** 1115–1137.

———, and others. 2006. An assessment of particulate organic carbon to thorium-234 ratios in the ocean and their impact on the application of ^{234}Th as a POC flux proxy. Mar. Chem. **100:** 213–233, doi:10.1016/j.marchem.2005.10.013

———, C. R. Benitez-Nelson, M. R. Van Der Loeff, J. E. Andrews, L. Ball, G. Crossin, and M. A. Charette. 2001. An intercomparison of small- and large-volume techniques for thorium-234 in seawater. Mar. Chem. **74:** 15–28, doi:10.1016/S0304-4203(00)00092-X

Calbet, A., and M. R. Landry. 2004. Phytoplankton growth, microzooplankton grazing, and carbon cycling in marine systems. Limnol. Oceanogr. **49:** 51–57, doi:10.4319/lo.2004.49.1.0051

Chen, J. H., R. L. Edwards, and G. J. Wasserburg. 1986. ^{238}U, ^{234}U and ^{232}Th in seawater. Earth Planet. Sci. Lett. **80:** 241–251, doi:10.1016/0012-821X(86)90108-1

Conover, R. J. 1966. Assimilation of organic matter by zooplankton. Limnol. Oceanogr. **11:** 338–345, doi:10.4319/lo.1966.11.3.0338

Dunne, J. P., R. A. Armstrong, A. Gnanadesikan, and J. L. Sarmiento. 2005. Empirical and mechanistic models for the particle export ratio. Glob. Biogeochem. Cycles **19:** GB4026, doi:10.1029/2004GB002390

Eppley, R. W., and B. J. Peterson. 1979. Particulate organic matter flux and planktonic new production in the deep ocean. Nature **282:** 677–680, doi:10.1038/282677a0

———, E. H. Renger, and W. G. Harrison. 1979. Nitrate and phytoplankton production in southern California coastal waters. Limnol. Oceanogr. **24:** 483–494, doi:10.4319/lo.1979.24.3.0483

Green, S. E., and R. N. Sambrotto. 2006. Plankton community structure and export of C, N, P and Si in the Antarctic Circumpolar Current. Deep-Sea Res. Part II **53:** 620–643, doi:10.1016/j.dsr2.2006.01.022

Gruber, N., and others. 2006. Eddy-resolving simulation of plankton ecosystem dynamics in the California Current System. Deep-Sea Res. Part I-Oceanogr. Res. Pap. **53:** 1483–1516, doi:10.1016/j.dsr.2006.06.005

Harrison, W. G., T. Platt, and M. R. Lewis. 1987. *f*-ratio and its relationship to ambient nitrate concentration in coastal waters. J. Plankton Res. **9:** 235–248, doi:10.1093/plankt/9.1.235

Jackson, G. A. 2001. Effect of coagulation on a model planktonic food web. Deep-Sea Res. Part I **48:** 95–123, doi:10.1016/S0967-0637(00)00040-6

Landry, M. R., and A. Calbet. 2004. Microzooplankton production in the oceans. ICES J. Mar. Sci. **61:** 501–507, doi:10.1016/j.icesjms.2004.03.011

———, C. J. Lorenzen, and W. K. Peterson. 1994. Mesozooplankton grazing in the Southern California Bight .2. Grazing impact and particulate flux. Mar. Ecol. Prog. Ser. **115:** 73–85, doi:10.3354/meps115073

———, M. D. Ohman, M. R. Stukel, and K. Tsyrklevich. 2009. Lagrangian studies of phytoplankton growth and grazing relationships in a coastal upwelling ecosystem off Southern California. Prog. Oceanogr. **83:** 208–216, doi:10.1016/j.pocean.2009.07.026

———, K. E. Selph, and E. J. Yang. 2011. Decoupled phytoplankton growth and microzooplankton grazing in the deep euphotic zone of the HNLC equatorial Pacific. Mar. Ecol. Prog. Ser. **421:** 13–24, doi:10.3354/meps08792

Lavaniegos, B. E., and M. D. Ohman. 2007. Coherence of long-term variations of zooplankton in two sectors of the California Current System. Prog. Oceanogr. **75:** 42–69, doi:10.1016/j.pocean.2007.07.002

Laws, E. A., P. G. Falkowski, W. O. Smith, H. Ducklow, and J. J. McCarthy. 2000. Temperature effects on export production in the open ocean. Glob. Biogeochem. Cycles **14:** 1231–1246, doi:10.1029/1999GB001229

Lynn, R. J., and J. J. Simpson. 1987. The California Current System: The seasonal variability of its physical characteristics. J. Geophys. Res. Oceans **92:** 12947–12966, doi:10.1029/JC092iC12p12947

Michaels, A. F., and M. W. Silver. 1988. Primary production, sinking fluxes and the microbial food web. Deep-Sea Res. **35:** 473–490.

Nelson, J. R., J. R. Beers, R. W. Eppley, G. A. Jackson, J. J. Mccarthy, and A. Soutar. 1987. A particle flux study in the Santa Monica-San Pedro Basin off Los Angeles: Particle flux, primary production, and transmissometer survey. Cont. Shelf Res. **7:** 307–328, doi:10.1016/0278-4343(87)90071-9

Olivieri, R. A., and F. P. Chavez. 2000. A model of plankton dynamics for the coastal upwelling system of Monterey Bay, California. Deep-Sea Res. Part II **47:** 1077–1106, doi:10.1016/S0967-0645(99)00137-X

Pike, S. M., K. O. Buesseler, J. Andrews, and N. Savoye. 2005. Quantification of ^{234}Th recovery in small volume sea water samples by inductively coupled plasma-mass spectrometry. J. Radioanal. Nucl. Chem. **263:** 355–360.

Plattner, G. K., N. Gruber, H. Frenzel, and J. C. Mcwilliams. 2005. Decoupling marine export production from new production. Geophys. Res. Lett. **32:** L11612, doi:10.1029/2005GL022660

Rodriguez Y Baena, A. M., M. Metian, J. L. Teyssie, C. De Broyer, and M. Warnau. 2006. Experimental evidence for ^{234}Th bioaccumulation in three Antarctic crustaceans: Potential implications for particle flux studies. Mar. Chem. **100:** 354–365, doi:10.1016/j.marchem.2005.10.022

Roemmich, D. 1992. Ocean warming and sea-level rise along the Southwest U.S. Coast. Science **257:** 373–375, doi:10.1126/science.257.5068.373

———, and J. McGowan. 1995. Climatic warming and the decline of zooplankton in the California Current. Science **267:** 1324–1326, doi:10.1126/science.267.5202.1324

Rykaczewski, R. R., and D. M. Checkley. 2008. Influence of ocean winds on the pelagic ecosystem in upwelling regions. Proc. Natl. Acad. Sci. U. S. A. **105:** 1965–1970, doi:10.1073/pnas.0711777105

Savoye, N., and others. 2006. ^{234}Th sorption and export models in the water column: A review. Mar. Chem. **100:** 234–249, doi:10.1016/j.marchem.2005.10.014

Siegel, D. A., T. C. Granata, A. F. Michaels, and T. D. Dickey. 1990. Mesoscale eddy diffusion, particle sinking, and the interpretation of sediment trap data. J. Geophys. Res. Oceans **95:** 5305–5311, doi:10.1029/JC095iC04p05305

Small, L. F., and S. G. Ellis. 1992. Fecal carbon production by zooplankton in Santa-Monica Basin: The effects of body size and carnivorous feeding. Prog. Oceanogr. **30:** 197–221, doi:10.1016/0079-6611(92)90013-P

Smayda, T. J. 1970. The suspension and sinking of phytoplankton in the sea. Oceanogr. Mar. Biol. Ann. Rev. **8:** 353–414.

Straile, D. 1997. Gross growth efficiencies of protozoan and metazoan zooplankton and their dependence on food concentration, predator–prey weight ratio, and taxonomic group. Limnol. Oceanogr. **42:** 1375–1385, doi:10.4319/lo.1997.42.6.1375

Turner, J. T. 2002. Zooplankton fecal pellets, marine snow and sinking phytoplankton blooms. Aquat. Microb. Ecol. **27:** 57–102, doi:10.3354/ame027057

Umani, S. F., and others. 2002. Particulate matter and plankton dynamics in the Ross Sea Polynya of Terra Nova Bay during the Austral Summer 1997/98. J. Mar. Syst. **36:** 29–49, doi:10.1016/S0924-7963(02)00133-1

Venrick, E. L. 1998. Spring in the California current: The distribution of phytoplankton species, April 1993 and April 1995. Mar. Ecol. Prog. Ser. **167:** 73–88, doi:10.3354/meps167073

———. 2002. Floral patterns in the California Current System off southern California: 1990–1996. J. Mar. Res. **60:** 171–189, doi:10.1357/002224002762341294

Walsh, I. D., and W. D. Gardner. 1992. A comparison of aggregate profiles with sediment trap fluxes. Deep-Sea Res. **39:** 1817–1834.

Associate editor: George W. Kling

Received: 09 September 2010
Accepted: 11 July 2011
Amended: 17 June 2011